Physica B 719 (2025) 417913

Contents lists available at ScienceDirect

Physica B: Condensed Matter

journal homepage: www.elsevier.com/locate/physb

Electronic structure of a *p*-type topological insulator $SnSbBiTe_4$

S.V. Eremeev [a,b], L. Ferrari [c], P.M. Sheverdyaeva [d], O. De Luca [e,f,g], T. Caruso [e,f], M. Casciaro [e,f], Kh.Z. Mehtiyeva [h], Z.S. Aliev [h,i], E.V. Chulkov [j,b], A.S. Vasenko [b], G. Di Santo [k], L. Petaccia [k], M. Papagno [e,f], D. Pacilé [e,f,*]

[a] Institute of Strength Physics and Materials Science of Siberian Branch of Russian Academy of Sciences, 634055 Tomsk, Russia
[b] HSE University, 101000 Moscow, Russia
[c] CNR-Istituto di Struttura della Materia (CNR-ISM), 00133 Roma, Italy
[d] CNR-Istituto di Struttura della Materia (CNR-ISM), SS 14, Km 163.5, 34149 Trieste, Italy
[e] Dipartimento di Fisica, Università della Calabria, Via P. Bucci, I-87036 Rende (CS), Italy
[f] Laboratorio di Spettroscopia Avanzata dei Materiali, STAR IR, Via Tito Flavio, Università della Calabria, 87036, Rende, CS, Italy
[g] CNR-Istituto di Nanotecnologia (CNR-Nanotec) - UoS Cosenza, 87036, Rende, CS, Italy
[h] Baku State University, AZ1148 Baku, Azerbaijan
[i] Institute of Physics, Science and Education Ministry of Azerbaijan, AZ1143 Baku, Azerbaijan
[j] Donostia International Physics Center, 20018 Donostia-San Sebastián, Spain
[k] Elettra Sincrotrone Trieste, Strada Statale 14 km 163.5, 34149 Trieste, Italy

ARTICLE INFO

Keywords:
Topological insulators
$SnSbBiTe_4$
ARPES
DFT

ABSTRACT

This study explores the bulk and surface electronic band structure of the $SnSbBiTe_4$ van der Waals (vdW) compound composed of septuple layer (SL) vdW blocks in which pnictogen atoms (Sb,Bi) share the same sublattice in a 50/50 ratio. We provide a characterization of the electronic structure of $SnSbBiTe_4$ by means of core-level photoemission spectroscopy and angle-resolved photoemission spectroscopy, complementing experimental studies with density functional theory calculations.

1. Introduction

Spintronic devices using topological insulators (TIs) are highly effective for spin-to-charge conversion, due to the presence of topologically protected surface states (TSSs) [1–3]. These states exhibit both Dirac-like dispersion and spin-momentum locking. The position of the Dirac point-where TSS branches intersect-and its interaction with bulk bands at the Fermi level (E_F) are key factors that influence whether the material exhibits topological or trivial transport behavior. Over recent decades, precise adjustments of the chemical composition of these materials have been extensively studied to control the E_F position relative to the Dirac surface state [4–6].

We focus on the $SnSbBiTe_4$ compound as a case study, to investigate the effects of a mixed SbBi (50/50) composition in comparison with $SnBi_2Te_4$ [7] and $SnSb_2Te_4$ [8], which are *n*- and *p*-doped TIs, respectively. The $SnSbBiTe_4$ compound has the same crystal structure as several layered van der Waals (vdW) TIs: $GeSb_2Te_4$, $GeBi_2Te_4$ [9,10], $SnSb_2Te_4$ [8,9,11], $SnBi_2Te_4$ [7,9], $PbBi_2Se_4$ [9], $PbBi_2Te_4$ [9,12], $PbSb_2Te_4$ [9,11], $PbBi_2Te_2Se_2$ [13], as well as their magnetic Mn-based counterparts $MnBi_2Te_4$ and $MnSb_2Te_4$ [14–17]. All of these compounds are composed of septuple layer blocks, each layer being element-specific, while, ideally, the pnictogen sublattice in $SnSbBiTe_4$ is uniformly occupied by Sb and Bi atoms (see Fig. 1a).

Topological insulators offer a versatile platform for studying quantum coherence and topological protection in low-dimensional systems [18–20]. The present study addresses an active area of interest in Bi–Sb-based TIs, driven by their robust surface states and the emergence of distinct quantum phenomena such as Aharonov–Bohm (AB) oscillations. In Bi–Sb-based TIs, by tuning the Bi/Sb ratio it is possible to engineer a bulk-insulating regime while preserving gapless, spin-momentum-locked surface states that are resilient to non-magnetic disorder. This makes Bi–Sb-based compounds promising candidates for applications in quantum information, spintronics, and low-dissipation electronics, and ideal systems for probing Berry-phase-related effects and quantum interference phenomena [21–23]. Interestingly, it was recently shown [22,24] that mixing Bi and Sb leads to higher magnetoresistance compared to the pure A_2B_3 (A = Sb or Bi; B = Se or Te) family of TIs. An open question that remains to be addressed concerns the effect of mixing of pnictogen atoms on the electronic structure of TIs and how such modifications influence the quantum properties of the material.

* Corresponding author.
E-mail address: daniela.pacile@fis.unical.it (D. Pacilé).

https://doi.org/10.1016/j.physb.2025.417913
Received 7 August 2025; Received in revised form 3 October 2025; Accepted 8 October 2025
Available online 1 November 2025

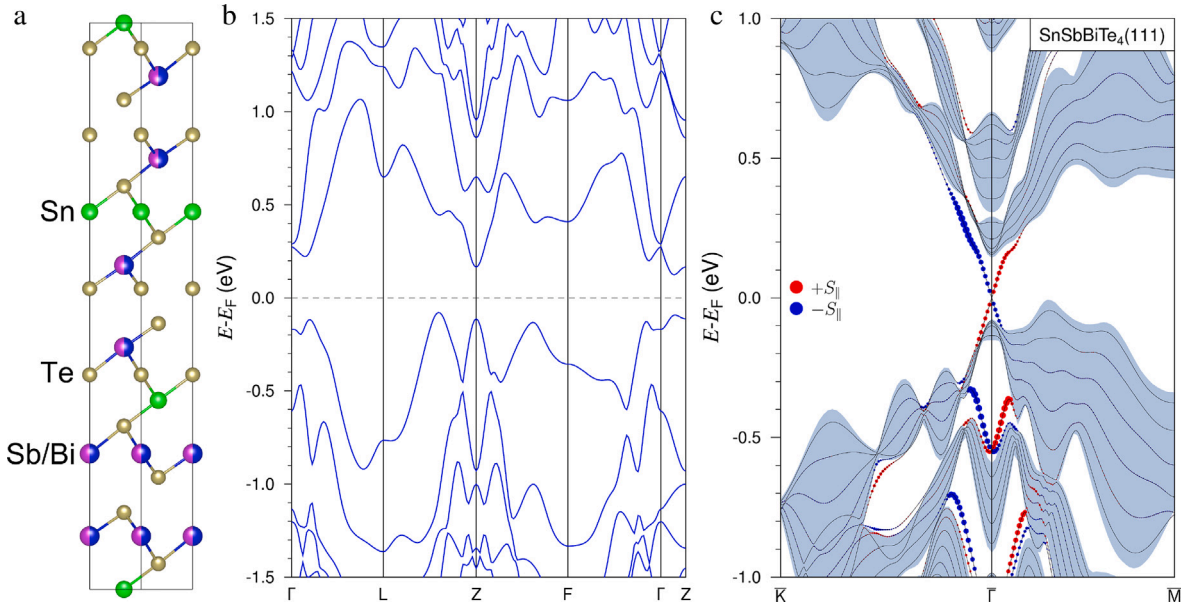

Fig. 1. (a) Crystal structure of $SnSbBiTe_4$ compound visualized with VESTA [29]. (b) Bulk band structure calculated within DFT-1/2 approach along high-symmetry directions of the bulk Brillouin zone of the primitive rhombohedral cell. (c) Surface spectrum of $SnSbBiTe_4$(111). Red/blue dots mark the positive/negative sign of the in-plane spin projections for spin-polarized surface states. Shaded areas correspond to projection of the bulk states onto the (111) plane.

In the present paper we provide a characterization of the $SnSbBiTe_4$ electronic structure using core-level photoemission spectroscopy (PES) and angle-resolved photoemission spectroscopy (ARPES). In analogy with the pure $SnSb_2Te_4$ compound [8], the experimental results reported here demonstrate a *p*-type doping of this TI, as opposed to the expected at Bi–Sb intermixing, bulk-insulating TI, similar to $(Bi–Sb)_2Te_3$ [25–28]. In addition, comparing the experimental band structure with the state-of-the-art simulations offers crucial insights into the intricate relationship between the position of E_F and the elemental composition. This complexity apparently arises from the defect compensation effect, which mitigates the *p*(*n*) doping in the original Sb(Bi)-based systems, becoming even more complicated when a IV group element is present in the compound.

2. Experimental methods

Single crystalline ingots of $SnSbBiTe_4$ were grown from nonstoichiometric composition by the vertical Bridgman–Stockbarger method [30]. The synthesis was performed in two steps. First, the polycrystalline composition was synthesized from high-purity (5N) elements in evacuated quartz ampule at about 1000 K for 8 h mixing incessantly, followed by air cooling. Afterward, the polycrystalline sample was placed in a conical-bottom quartz ampule, which was sealed under a vacuum better than 10^{-6} mbar. At the beginning of the growing process, the ampule was held in the "hot" zone (≈920 K) of a two-zone tube furnace for 24 h for a complete melting of the composition. The charged ampule moves from the "hot" zone to the "cold" zone with the required rate 1.0 mm/h. In this way, bulk ingot with average dimensions of ≈4 cm in length and 0.8 cm in diameter was obtained.

The powder X-ray diffraction pattern (PXRD) for the $SnSbBiTe_4$ compound is given in Fig. S1 of the Supplementary file. As can be seen, it has a qualitatively identical diffraction pattern to that of parent $SnSb_2Te_4$ (a) and $SnBi_2Te_4$ (c) compounds. The negligible shifting in the peak positions from $SnBi_2Te_4$ to $SnSb_2Te_4$ towards high angles confirms the ternary solubility of bismuth and antimony in the septuple units of both parent compounds. The lack of diffraction lines of the elemental Sb and Bi in the PXRD pattern of the $SnSbBiTe_4$ alloy further confirms the starting 50:50 ratio of Sb and Bi in the grown single crystal.

The photoemission measurements were performed on surfaces obtained by cleavage at room-temperature in ultrahigh-vacuum (UHV) conditions. The cleaved surfaces were stable for several days in UHV. The high-quality single-crystalline (0001) surface was verified by the sharp features in the Low Energy Electron Diffraction (LEED) pattern (see inset of Fig. 2a). The chemical composition of TIs samples has been checked by core-level measurements, carried out at the VUV-Photoemission beamline of the Elettra synchrotron light laboratory. Low energy ARPES measurements were carried out at the BaDElPh beamline [31] of Elettra at 80 K, with energy resolution of about 20 meV and momentum resolution of ~0.02 $Å^{-1}$. Rubidium was sublimated in UHV (in the 10^{-10} mbar range) by using commercial SAES getter dispensers, after overnight degassing at currents slightly below the sublimation onset. The deposition of alkali metal on the pristine TI was repeated until the saturation in electron doping was achieved.

3. Computational details

The electronic structure calculations were carried out within the framework of density functional theory (DFT) using the VASP code [32,33]. The projected augmented wave (PAW) method was used in the calculation scheme [34,35]. The generalized gradient approximation (GGA) as formulated by Perdew–Burke–Ernzerhof (PBE) [36] was used for the exchange–correlation potential. Relativistic effects were taken into account, including the spin–orbit interaction (SOI).

The accurate cell parameters and atomic positions of $SnSb_2Te_4$ and $SnBi_2Te_4$ bulk cells were obtained using VASP's built-in conjugate gradient algorithm. The first Brillouin zone (BZ) of the primitive rhombohedral cells of $SnSb_2Te_4$ and $SnBi_2Te_4$ was sampled by the 8 × 8 × 8 Γ-centered Monkhorst–Pack grid and the occupations of electronic states were smeared according to Gaussian function of width of 10 meV. The vdW corrections were taken into account using the DFT-D3 functional with Becke–Johnson dumping scheme [37]. The geometry optimization was performed until the residual forces on atoms became smaller than 1 meV/Å. The combination of GGA and vDW functionals usually gives reliable results for the equilibrium structure of Bi_2Te_3-type layered materials, see for example Ref. [38].

The Bi-Sb site intermixing in $SnSbBiTe_4$ was simulated by means of the virtual crystal approximation (VCA) [39]. Lattice constants and

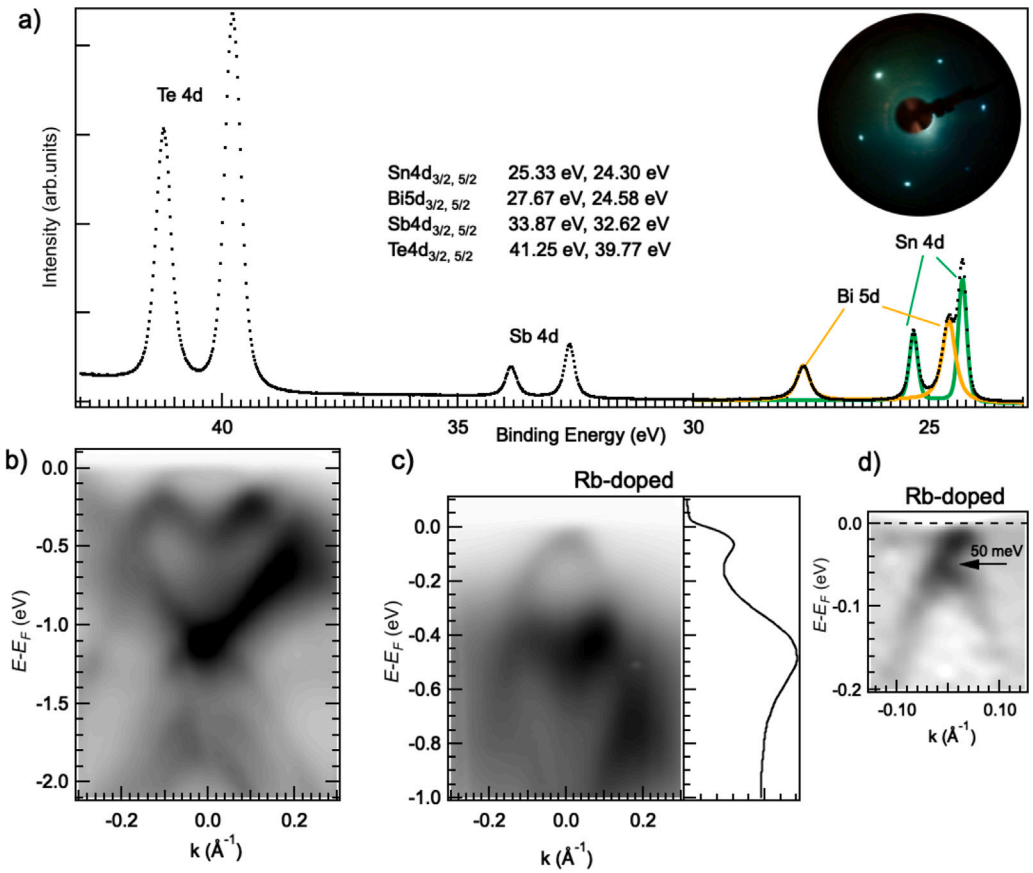

Fig. 2. (a) Photoemission measurements of $SnSbBiTe_4$ measured with 70 eV photon energy. In the inset, a LEED image showing the hexagonal symmetry at surface is reported. (b) Energy–momentum dispersion along $\bar{\Gamma}$-$\bar{M}$ of the first SBZ of $SnSbBiTe_4$, taken at 17 eV photon energy. (c) Same as (b), after Rb deposition. On the right, energy distribution curve extracted at $\bar{\Gamma}$, showing the position of the TSS with respect to the Rashba spin-split surface band. (d) Crossing of the TSS in Rb-doped sample.

interlayer distances in this case were calculated from equilibrium structures of $SnSb_2Te_4$ and $SnBi_2Te_4$ in accordance with the Vegard's law. The surface was not relaxed, which is reasonable when both parent phases in the equilibrium state are topological insulators, in contrast to instances where the topological phase develops only under strain, as is the case with the As_2Te_3 compound [40].

For accurate band structure calculations we apply the Slater-type DFT-1/2 self-energy correction method [41,42] which only requires the addition of a self-energy correction potential, calculated from a partially ionized free atom, to the standard DFT potential. In this case, the ionization level ($-1/2e$ by default) can be an additional variable parameter for fitting the band structure. This semiempirical quasiparticle scheme yields accurate band structures for many semiconductors and TIs [43] and owing to its low computational cost DFT-1/2 can be considered as a good alternative to expensive and time consuming computational approaches like GW. For $SnSbBiTe_4$ compound the quaternary ionization (-0.25 e) of tellurium and pnictogen atoms potentials was applied.

The $SnSbBiTe_4$(111) surface was simulated within a model of repeating slabs separated by a vacuum gap of 11 Å with the slab thickness of six septuple layers (SLs). The 2D BZ was sampled with the $10 \times 10 \times 1$ k-mesh.

4. Results

The $SnSbBiTe_4$ topological insulator crystallizes in a trigonal structure with hexagonal unit cell, where septuple-layer blocks [Te–Sb/Bi–Te–Sn–Te–Sb/Bi–Te] are stacked along the vertical axis, as shown in Fig. 1a. The bonds inside the septuple layer have mainly an ionic–covalent character, whereas the blocks are held together by weak vdW forces [44].

The bulk band spectrum calculated along high-symmetry directions of the Brillouin zone of primitive rhombohedral cell is demonstrated in Fig. 1b. To calculate the band structure we firstly adjusted the potentials within DFT-1/2 method [41,42] by searching an extremum of the Z point gap (the point in which the SOI-induced band inversion occurs) by variation of the cutoff radius r_{cut} in spherical step function multiplier for atomic self-energy potential. Earlier it was shown for XSb_4Te_4 compounds (X = Ge, Sn, Pb) [45] that it is sufficient to construct the potentials for pnictogen and halogen atoms to describe the band structure accurately while the potential of carbon group X element does not affect the bands near E_F. For $SnSbBiTe_4$ we also left the original Sn potential, and variation of r_{cut} for Bi and Sb potentials was carried out simultaneously within the framework of the VCA. The resulting r_{cut} were found to be 3.78 and 3.90 a.u. (2.00 and 2.06 Å) for Te and Sb/Bi potentials, respectively. Within this approach the bulk gap was found to be of 205 meV. This gap is indirect with conduction band minimum (CBM) in the middle of the Γ-Z and valence band maximum (VBM) laying along L-Z direction. According to calculations the products of wave functions parities [46] at Γ, Z and $F_{1,2,3}$ points they are equal to -1, while those at $L_{1,2,3}$ points are $+1$ and hence the Z2 topological invariant $(\nu_0; \nu_1\nu_2\nu_3)$ in $SnSbBiTe_4$ is (1;000). On the projection of the bulk states onto the (111) cleavage surface the CBM extremum appears at the $\bar{\Gamma}$ point of the 2D Brillouin zone, while the VBM occurs at ~1/4 of $\bar{\Gamma}$-$\bar{M}$ direction (Fig. 1c).

The surface spectrum of $SnSbBiTe_4$ possesses a spin-helical TSS with the Dirac dispersion within the gap which deviates from linear

behavior only approaching the conduction band and its crossing point lies approximately in the middle of the gap, far from both VBM and CBM. In addition to the Dirac state, the surface spectrum also contains a prominent Rashba spin-split surface band in the local band gap of the valence band at ≈ −0.5 eV at the $\bar{\Gamma}$ point that is typical for all vdW-structured TIs and first shown for Sb_2Te_3 [47].

From an experimental point of view, we characterize the chemical composition of $SnSbBiTe_4$ by means of core-level photoemission, with representative spectra shown in Fig. 2a, taken at a photon energy of 70 eV. The core-level peaks expected in this energy range are detected and listed in the graph. The quantitative analysis of all peaks is complex due to the septuple-layer structure composed of element-specific single layers, the signal attenuation caused by the inelastic mean free path of photoelectrons, and the diffraction effects seen at the photon energy used. In Fig. S2 of the Supplementary file, we show a comparison with core-level spectra of $SnSb_2Te_4$ and $SnBi_2Te_4$, measured under the same experimental conditions. The variation in peaks intensity is consistent with the different chemical composition, and a total shift of about 200 meV towards lower binding energy is observed for the Te 4*d* peaks when going from $SnSb_2Te_4$ to $SnBi_2Te_4$, with $SnSbBiTe_4$ lying between.

In Fig. 2b–c, we show ARPES data acquired at a photon energy of 17 eV along the $\bar{\Gamma}$ -$\bar{M}$ direction of the first Surface Brillouin Zone (SBZ), measured on pristine and Rb-doped TIs, respectively. In both photoemission images we can observe sharp surface states and broad bulk bands. Electron doping moves all bands that lie close to E_F of (130 ± 20) meV. The Dirac surface state clearly emerges after Rb doping (Fig. 2c), with a Dirac point at ≈ −0.5 eV from the prominent Rashba spin-split surface band, in good agreement with Fig. 1c. This is also seen in the energy distribution curve extracted at $\bar{\Gamma}$ and reported on the right side of Fig. 2c. In Fig. 2d, we identify the crossing of the TSS and estimate the Dirac point at about 50 meV from E_F for the selected Rb-doping.

By comparing the photoemission images of pristine and Rb-doped TIs, taking into account a rigid band shift of about 130 meV (Fig. 2b–c), we estimate a Dirac point in pristine $SnSbBiTe_4$ at about 80 meV. This also corresponds to the energy offset observed between theoretical calculations and experimental results. Notably, the Dirac point was reported at 300 meV above E_F in $SnSb_2Te_4$ [8], whereas in $SnBi_2Te_4$ it is shifted to 360 meV below E_F, within the occupied states [7].

The offset of about 80 meV between the predicted and experimental Dirac point position of the TSS can be attributed to several factors. On the one hand, it may result from possible stoichiometric inhomogeneities of Sb-Bi across the sample volume, which are expected in crystals grown by the Bridgman method. However, multiple cleaves of different ingots systematically showed *p*-type doping, suggesting that such inhomogeneities might be an intrinsic feature rather than a local fluctuation. On the other hand, the defect compensation mechanism may not be effective in this case.

To explain why in the $SnSbBiTe_4$ compound when Bi and Sb are mixed, the *p*-type and *n*-type defects do not compensate each other, we need to turn to the physics of defects in quintuple-layered binary V_2VI_3 compounds where they were studied in detail [48–53]. As was shown, the *p*−*n* crossover and carrier concentration in this kind of materials can be governed by alloying on either V (Bi-Sb) or VI (Te-Se) sublattices. It was pointed that there is a correlation between the conduction type and the carrier concentration of intrinsic point defects and the electronegativity and covalent radius of cations and anions [52].

In particular, in Bi_2Se_3 the selenium vacancies are the dominant donor defects, which are responsible for unintentional *n*-type conductivity in this material [50]. In contrast, in Bi_2Te_3 the anti-sites are dominant defects. Under Bi-poor conditions the Te_{Bi} anti-site donor defect has the lowest formation energy that yields *n*-type conductivity while under Bi-rich conditions the acceptor Bi anti-site defect, Bi_{Te}, becomes preferred promoting a tendency for *p*-type conductivity [50]. Since the concentration of different types of defects depends not only on the growth conditions but also has a tendency to vary with different positions in the crystal boule [52], this allows to realize the $p-n$ transition in the single Bi_2Te_3 crystal [51]. It was demonstrated that alloying Bi_2Se_3 and Bi_2Te_3 with formation Bi_2Te_2Se and $Bi_2Te_{2.5}Se_{0.5}$ compounds results in the *p*-type and *n*-type defects compensation and formation of the intrinsic TI phases where only the TSS intersects E_F [50]. However, such compensations does not occur in septuple-layered $PbBi_2Te_{4-x}Se_x$ compounds [13] which remain *n*-type TIs at different alloying ($x = 2, 2.6$).

Natural Sb_2Te_3 exhibits a strong *p*-type conductivity, which is related to negatively charged Sb vacancies and Sb_{Te} anti-sites [49,52,54,55]. The possibility of achieving the intrinsic TI state with isovalent Sb-Bi substitution with formation of $Bi_xSb_{2-x}Te_3$ compounds at Bi:Sb ratio close to 1:1 has been repeatedly demonstrated by ARPES and transport measurements [27,28,56,57]. However, in $SnBiSbTe_4$ such compensation of *p*-type and *n*-type defects does not occur. Thus, in the $IV_1V_2VI_4$ compound $SnBiSbTe_4$, like in $PbBi_2Te_{4-x}Se_x$ [13], the donor- and acceptor-type defects balance must take into account the presence of charged defects on the IV group sublattice, both vacancies and anti-sites, while compensation of *p*-type and *n*-type defects on the pnictogen and chalcogen sublattices is not sufficient to change the type of conductivity in these materials.

5. Conclusions

The $SnSbBiTe_4$ compound is confirmed to be a *p*-type TI exhibiting well-defined TSS, as demonstrated by ARPES measurements and supported by advanced DFT calculations. Despite the equal mixing of Sb and Bi atoms on the pnictogen sublattice, no compensation between donor- and acceptor-type defects is observed, resulting in a persistent *p*-type character. The Dirac point resides within the bulk energy gap, consistent with a robust TSS. The agreement between experimental data and DFT-1/2 simulations highlights the effectiveness of this computational approach for modeling the electronic structure of complex vdW layered systems. These findings not only deepen our understanding of defect-driven doping mechanisms in layered TIs but also suggest that the design of multi-component IV–V–VI compounds offers a promising strategy for engineering topological materials.

CRediT authorship contribution statement

S.V. Eremeev: Writing – review & editing, Methodology, Formal analysis, Conceptualization. **L. Ferrari:** Writing – review & editing, Investigation, Formal analysis, Data curation. **P.M. Sheverdyaeva:** Writing – review & editing, Investigation, Formal analysis, Data curation. **O. De Luca:** Investigation, Data curation. **T. Caruso:** Investigation, Data curation. **M. Casciaro:** Formal analysis, Data curation. **Kh.Z. Mehtiyeva:** Resources, Investigation, Data curation. **Z.S. Aliev:** Writing – review & editing, Resources, Investigation. **E.V. Chulkov:** Writing – review & editing, Funding acquisition. **A.S. Vasenko:** Formal analysis, Data curation. **G. Di Santo:** Investigation, Formal analysis, Data curation. **L. Petaccia:** Writing – review & editing, Supervision, Resources. **M. Papagno:** Writing – review & editing, Formal analysis, Data curation. **D. Pacilé:** Writing – review & editing, Writing – original draft, Investigation, Formal analysis.

Declaration of competing interest

The authors declare that they have no known competing financial interests or personal relationships that could have appeared to influence the work reported in this paper.

Acknowledgments

We acknowledge Elettra Sincrotrone Trieste for providing access to its synchrotron radiation facilities and for financial support under the SUI internal project. This research was supported in part by the Progetto STAR 2 (PIR01-00008) of the Italian Ministry of Education, University, and Research. S.V.E. acknowledges the support by the Government research assignment for ISPMS SB RAS (project FWRW-2022-0001) and Basic Research Program of the HSE University. The computational resources for this research were provided by the HPC facilities at HSE University. G.D.S. acknowledges the support by the Consortium INSTM (internal project TRI.25/068). We acknowledge EUROFEL ROADMAP ESFRI of the Italian Ministry of Education, University, and Research.

Appendix A. Supplementary data

Supplementary material related to this article can be found online at https://doi.org/10.1016/j.physb.2025.417913.

Data availability

No data was used for the research described in the article.

References

[1] K. Kondou, R. Yoshimi, A. Tsukazaki, Y. Fukuma, J. Matsuno, K.S. Takahashi, M. Kawasaki, Y. Tokura, Y. Otani, Fermi-level-dependent charge-to-spin current conversion by Dirac surface states of topological insulators, Nat. Phys. 12 (11) (2016) 1027–1031, http://dx.doi.org/10.1038/nphys3833.

[2] K.-S. Lin, G. Palumbo, Z. Guo, Y. Hwang, J. Blackburn, D.P. Shoemaker, F. Mahmood, Z. Wang, G.A. Fiete, B.J. Wieder, B. Bradlyn, Spin-resolved topology and partial axion angles in three-dimensional insulators, Nat. Commun. 15 (1) (2024) 550, http://dx.doi.org/10.1038/s41467-024-44762-w.

[3] J. Han, A. Richardella, S.A. Siddiqui, J. Finley, N. Samarth, L. Liu, Room-temperature spin-orbit torque switching induced by a topological insulator, Phys. Rev. Lett. 119 (2017) 077702, http://dx.doi.org/10.1103/PhysRevLett.119.077702, URL https://link.aps.org/doi/10.1103/PhysRevLett.119.077702.

[4] E. Rongione, S. Fragkos, L. Baringthon, J. Hawecker, E. Xenogiannopoulou, P. Tsipas, C. Song, M. Mičica, J. Mangeney, J. Tignon, T. Boulier, N. Reyren, R. Lebrun, J.-M. George, P. Le Fèvre, S. Dhillon, A. Dimoulas, H. Jaffrès, Ultrafast spin-charge conversion at $SnBi_2Te_4$/Co topological insulator interfaces probed by terahertz emission spectroscopy, Adv. Opt. Mater. 10 (7) (2022) 2102061, http://dx.doi.org/10.1002/adom.202102061.

[5] S. Fragkos, L. Baringthon, P. Tsipas, E. Xenogiannopoulou, P. Le Fèvre, P. Kumar, H. Okuno, N. Reyren, A. Lemaitre, G. Patriarche, J.-M. George, A. Dimoulas, Topological surface states in epitaxial $(SnBi_2Te_4)_n(Bi_2Te_3)_m$ natural van der Waals superlattices, Phys. Rev. Mater. 5 (2021) 014203, http://dx.doi.org/10.1103/PhysRevMaterials.5.014203, URL https://link.aps.org/doi/10.1103/PhysRevMaterials.5.014203.

[6] I. Grimaldi, D. Pacilè, S.V. Eremeev, O. De Luca, A. Policicchio, P. Moras, P.M. Sheverdyaeva, A.K. Kundu, Z.S. Aliev, P. Rudolf, R.G. Agostino, E.V. Chulkov, M. Papagno, Electronic band structure of three-dimensional topological insulators with different stoichiometry composition, Phys. Rev. B 102 (2020) 085118, http://dx.doi.org/10.1103/PhysRevB.102.085118, URL https://link.aps.org/doi/10.1103/PhysRevB.102.085118.

[7] S.V. Eremeev, O. De Luca, P.M. Sheverdyaeva, L. Ferrari, A.V. Matetskiy, G. Di Santo, L. Petaccia, C. Crovara, T. Caruso, M. Papagno, R.G. Agostino, Z.S. Aliev, P. Moras, C. Carbone, E.V. Chulkov, D. Pacilè, Energy-overlap of the Dirac surface state with bulk bands in $SnBi_2Te_4$, Phys. Rev. Mater. 7 (2023) 014203, http://dx.doi.org/10.1103/PhysRevMaterials.7.014203, URL https://link.aps.org/doi/10.1103/PhysRevMaterials.7.014203.

[8] D. Niesner, S. Otto, V. Hermann, T. Fauster, T.V. Menshchikova, S.V. Eremeev, Z.S. Aliev, I.R. Amiraslanov, M.B. Babanly, P.M. Echenique, E.V. Chulkov, Bulk and surface electron dynamics in a *p*-type topological insulator $SnSb_2$ Te_4, Phys. Rev. B 89 (2014) 081404, http://dx.doi.org/10.1103/PhysRevB.89.081404, URL https://link.aps.org/doi/10.1103/PhysRevB.89.081404.

[9] S.V. Eremeev, G. Landolt, T.V. Menshchikova, B. Slomski, Y.M. Koroteev, Z.S. Aliev, M.B. Babanly, J. Henk, A. Ernst, L. Patthey, A. Eich, A.A. Khajetoorians, J. Hagemeister, O. Pietzsch, J. Wiebe, R. Wiesendanger, P.M. Echenique, S.S. Tsirkin, I.R. Amiraslanov, J.H. Dil, E.V. Chulkov, Atom-specific spin mapping and buried topological states in a homologous series of topological insulators, Nat. Commun. 3 (1) (2012) 635, http://dx.doi.org/10.1038/ncomms1638.

[10] K. Okamoto, K. Kuroda, H. Miyahara, K. Miyamoto, T. Okuda, Z.S. Aliev, M.B. Babanly, I.R. Amiraslanov, K. Shimada, H. Namatame, M. Taniguchi, D.A. Samorokov, T.V. Menshchikova, E.V. Chulkov, A. Kimura, Observation of a highly spin-polarized topological surface state in $GeBi_2Te_4$, Phys. Rev. B 86 (2012) 195304, http://dx.doi.org/10.1103/PhysRevB.86.195304, URL https://link.aps.org/doi/10.1103/PhysRevB.86.195304.

[11] T.V. Menshchikova, S.V. Eremeev, E.V. Chulkov, Electronic structure of $SnSb_2Te_4$ and $PbSb_2Te_4$ topological insulators, Appl. Surf. Sci. 267 (2013) 1–3, URL https://www.sciencedirect.com/science/article/pii/S0169433212006903.

[12] K. Kuroda, H. Miyahara, M. Ye, S.V. Eremeev, Y.M. Koroteev, E.E. Krasovskii, E.V. Chulkov, S. Hiramoto, C. Moriyoshi, Y. Kuroiwa, K. Miyamoto, T. Okuda, M. Arita, K. Shimada, H. Namatame, M. Taniguchi, Y. Ueda, A. Kimura, Experimental verification of $PbBi_2Te_4$ as a 3D topological insulator, Phys. Rev. Lett. 108 (2012) 206803, http://dx.doi.org/10.1103/PhysRevLett.108.206803, URL https://link.aps.org/doi/10.1103/PhysRevLett.108.206803.

[13] I.A. Shvets, I.I. Klimovskikh, Z.S. Aliev, M.B. Babanly, J. Sánchez-Barriga, M. Krivenkov, A.M. Shikin, E.V. Chulkov, Impact of stoichiometry and disorder on the electronic structure of the $PbBi_2Te_{4-x}Se_x$ topological insulator, Phys. Rev. B 96 (2017) 235124, http://dx.doi.org/10.1103/PhysRevB.96.235124, URL https://link.aps.org/doi/10.1103/PhysRevB.96.235124.

[14] S.V. Eremeev, M.M. Otrokov, E.V. Chulkov, Competing rhombohedral and monoclinic crystal structures in $MnPn_2Ch_4$ compounds: An ab-initio study, J. Alloys Compd. 709 (2017) 172–178, URL https://www.sciencedirect.com/science/article/pii/S0925838817309015.

[15] M.M. Otrokov, I.I. Klimovskikh, H. Bentmann, D. Estyunin, A. Zeugner, Z.S. Aliev, S. Gaß, A.U.B. Wolter, A.V. Koroleva, A.M. Shikin, M. Blanco-Rey, M. Hoffmann, I.P. Rusinov, A.Y. Vyazovskaya, S.V. Eremeev, Y.M. Koroteev, V.M. Kuznetsov, F. Freyse, J. Sánchez-Barriga, I.R. Amiraslanov, M.B. Babanly, N.T. Mamedov, N.A. Abdullayev, V.N. Zverev, A. Alfonsov, V. Kataev, B. Büchner, E.F. Schwier, S. Kumar, A. Kimura, L. Petaccia, G. Di Santo, R.C. Vidal, S. Schatz, K. Kißner, M. Ünzelmann, C.H. Min, S. Moser, T.R.F. Peixoto, F. Reinert, A. Ernst, P.M. Echenique, A. Isaeva, E.V. Chulkov, Prediction and observation of an antiferromagnetic topological insulator, Nature 576 (7787) (2019) 416–422, URL https://doi.org/10.1038/s41586-019-1840-9.

[16] S.V. Eremeev, I.P. Rusinov, Y.M. Koroteev, A.Y. Vyazovskaya, M. Hoffmann, P.M. Echenique, A. Ernst, M.M. Otrokov, E.V. Chulkov, Topological magnetic materials of the $(MnSb_2Te_4)\cdot(Sb_2Te_3)_n$ van der Waals compounds family, J. Phys. Chem. Lett. 12 (17) (2021) 4268–4277, http://dx.doi.org/10.1021/acs.jpclett.1c00875.

[17] D.A. Glazkova, D.A. Estyunin, I.I. Klimovskikh, T.P. Makarova, O.E. Tereshchenko, K.A. Kokh, V.A. Golyashov, A.V. Koroleva, A.M. Shikin, Electronic Structure of Magnetic Topological Insulators Mn(Bi1 –xSbx)2Te4 with Various Concentration of Sb Atoms, JETP Lett. 115 (5) (2022) 286–291, http://dx.doi.org/10.1134/S0021364022100083.

[18] H.-S. Kim, T.-H. Hwang, N.-H. Kim, Y. Hou, D. Yu, H.S. Sim, Y.-J. Doh, Adjustable quantum interference oscillations in Sb-doped Bi2Se3 topological insulator nanoribbons, in: ACS Nano, ACS Nano 14 (10) (2020) 14118—14125, URL https://doi.org/10.1021/acsnano.0c06892.

[19] H. Peng, K. Lai, D. Kong, S. Meister, Y. Chen, X.-L. Qi, S.-C. Zhang, Z.-X. Shen, Y. Cui, Aharonov–Bohm interference in topological insulator nanoribbons, Nat. Mater. 9 (3) (2010) 225–229, http://dx.doi.org/10.1038/nmat2609.

[20] J.H. Bardarson, P.W. Brouwer, J.E. Moore, Aharonov-Bohm oscillations in disordered topological insulator nanowires, Phys. Rev. Lett. 105 (2010) 156803, http://dx.doi.org/10.1103/PhysRevLett.105.156803, URL https://link.aps.org/doi/10.1103/PhysRevLett.105.156803.

[21] D. Kumar, K. Kumar, N.K. Karn, G. Gurjar, V.P.S. Awana, Sudesh, Crystal growth & physical property characterization of mixed topological insulator $BiSbTe_3$, J. Mater. Sci., Mater. Electron. 36 (17) (2025) 1049, http://dx.doi.org/10.1007/s10854-025-15083-5.

[22] S.-M. Huang, P.-C. Wang, C. Lin, S.-Y. You, W.-C. Lin, L.-J. Lin, Y.-J. Yan, S.-H. Yu, M.C. Chou, The Aharonov-Bohm oscillation in the $BiSbTe_3$ topological insulator macroflake, Appl. Phys. Lett. 112 (20) (2018) 203103, http://dx.doi.org/10.1063/1.5023812.

[23] S.-M. Huang, C. Lin, S.-Y. You, Y.-J. Yan, S.-H. Yu, M. Chou, The quantum oscillations in different probe configurations in the $BiSbTe_3$ topological insulator macroflake, Sci. Rep. 12 (1) (2022) 5191, http://dx.doi.org/10.1038/s41598-022-09073-4.

[24] S.-M. Huang, S.-H. Yu, M. Chou, Two-carrier transport-induced extremely large magnetoresistance in high mobility Sb_2Se_3, J. Appl. Phys. 121 (1) (2017) 015107, http://dx.doi.org/10.1063/1.4973343.

[25] C. Niu, Y. Dai, Y. Zhu, Y. Ma, L. Yu, S. Han, B. Huang, Realization of tunable Dirac cone and insulating bulk states in topological insulators (Bi1,àíxSbx)2Te3, Sci. Rep. 2 (1) (2012) 976, http://dx.doi.org/10.1038/srep00976.

[26] R. Yoshimi, A. Tsukazaki, Y. Kozuka, J. Falson, K.S. Takahashi, J.G. Checkelsky, N. Nagaosa, M. Kawasaki, Y. Tokura, Quantum hall effect on top and bottom surface states of topological insulator (Bi1,àíxSbx)2Te3 films, Nat. Commun. 6 (1) (2015) 6627, http://dx.doi.org/10.1038/ncomms7627.

[27] D. Kong, Y. Chen, J.J. Cha, Q. Zhang, J.G. Analytis, K. Lai, Z. Liu, S.S. Hong, K.J. Koski, S.-K. Mo, Z. Hussain, I.R. Fisher, Z.-X. Shen, Y. Cui, Ambipolar field effect in the ternary topological insulator $(Bi_xSb_{1-x})_2Te_3$ by composition tuning, Nature Nanotechnology 6 (11) (2011) 705–709, http://dx.doi.org/10.1038/nnano.2011.172.

[28] J. Zhang, C.-Z. Chang, Z. Zhang, J. Wen, X. Feng, K. Li, M. Liu, K. He, L. Wang, X. Chen, Q.-K. Xue, X. Ma, Y. Wang, Band structure engineering in $(Bi_{1-x}Sb_x)_2Te_3$ ternary topological insulators, Nat. Commun. 2 (1) (2011) 574, http://dx.doi.org/10.1038/ncomms1588.

[29] K. Momma, F. Izumi, *VESTA 3* for three-dimensional visualization of crystal, volumetric and morphology data, J. Appl. Crystallogr. 44 (6) (2011) 1272–1276, http://dx.doi.org/10.1107/S0021889811038970.

[30] D. Niesner, S. Otto, V. Hermann, T. Fauster, T.V. Menshchikova, S.V. Eremeev, Z.S. Aliev, I.R. Amiraslanov, M.B. Babanly, P.M. Echenique, E.V. Chulkov, Bulk and surface electron dynamics in a *p*-type topological insulator $SnSb_2Te_4$, Phys. Rev. B 89 (2014) 081404, http://dx.doi.org/10.1103/PhysRevB.89.081404, URL https://link.aps.org/doi/10.1103/PhysRevB.89.081404.

[31] L. Petaccia, P. Vilmercati, S. Gorovikov, M. Barnaba, A. Bianco, D. Cocco, C. Masciovecchio, A. Goldoni, BaD ElPh: A 4m normal-incidence monochromator beamline at Elettra, Nucl. Instrum. Methods Phys. Res. A 606 (3) (2009) 780–784, http://dx.doi.org/10.1016/j.nima.2009.05.001, URL https://www.sciencedirect.com/science/article/pii/S0168900209009127.

[32] G. Kresse, J. Hafner, Ab initio molecular dynamics for open-shell transition metals, Phys. Rev. B 48 (1993) 13115–13118, http://dx.doi.org/10.1103/PhysRevB.48.13115, URL https://link.aps.org/doi/10.1103/PhysRevB.48.13115.

[33] G. Kresse, J. Furthmüller, Efficiency of ab-initio total energy calculations for metals and semiconductors using a plane-wave basis set, Comput. Mater. Sci. 6 (1) (1996) 15–50, URL https://www.sciencedirect.com/science/article/pii/0927025696000080.

[34] P.E. Blöchl, Projector augmented-wave method, Phys. Rev. B 50 (1994) 17953–17979, http://dx.doi.org/10.1103/PhysRevB.50.17953, URL https://link.aps.org/doi/10.1103/PhysRevB.50.17953.

[35] G. Kresse, D. Joubert, From ultrasoft pseudopotentials to the projector augmented-wave method, Phys. Rev. B 59 (1999) 1758–1775, http://dx.doi.org/10.1103/PhysRevB.59.1758, URL https://link.aps.org/doi/10.1103/PhysRevB.59.1758.

[36] J.P. Perdew, K. Burke, M. Ernzerhof, Generalized gradient approximation made simple, Phys. Rev. Lett. 77 (1996) 3865–3868, http://dx.doi.org/10.1103/PhysRevLett.77.3865, URL https://link.aps.org/doi/10.1103/PhysRevLett.77.3865.

[37] S. Grimme, S. Ehrlich, L. Goerigk, Effect of the damping function in dispersion corrected density functional theory, J. Comput. Chem. 32 (7) (2011) 1456–1465, http://dx.doi.org/10.1002/jcc.21759, URL https://onlinelibrary.wiley.com/doi/abs/10.1002/jcc.21759.

[38] T.K. Reid, S.P. Alpay, A.V. Balatsky, S.K. Nayak, First-principles modeling of binary layered topological insulators: structural optimiza- tion and exchange-correlation functionals, Phys. Rev. B 101 (2020) 085140, http://dx.doi.org/10.1103/PhysRevB.101.085140.

[39] L. Bellaiche, D. Vanderbilt, Virtual crystal approximation revisited: Application to dielectric and piezoelectric properties of perovskites, Phys. Rev. B 61 (2000) 7877–7882, http://dx.doi.org/10.1103/PhysRevB.61.7877, URL https://link.aps.org/doi/10.1103/PhysRevB.61.7877.

[40] T.K. Reid, S.K. Nayak, S.P. Alpay, Strain-induced surface modali- ties in pnictogen chalcogenide topological insulators, J. Appl. Phys. 129 (1) (2021) 015304, http://dx.doi.org/10.1063/5.0028231.

[41] L.G. Ferreira, M. Marques, L.K. Teles, Approximation to density functional theory for the calculation of band gaps of semiconductors, Phys. Rev. B 78 (2008) 125116, http://dx.doi.org/10.1103/PhysRevB.78.125116, URL https://link.aps.org/doi/10.1103/PhysRevB.78.125116.

[42] L.G. Ferreira, M. Marques, L.K. Teles, Slater half-occupation technique revisited: the LDA-1/2 and GGA-1/2 approaches for atomic ionization energies and band gaps in semiconductors, AIP Adv. 1 (3) (2011) 032119, http://dx.doi.org/10.1063/1.3624562.

[43] T. Mota, F. Matusalem, M. Marques, L.K. Teles, I. Guilhon, DFT-1/2 method applied to 3D topological insulators, J. Phys.: Condens. Matter. 34 (46) (2022) 465501, http://dx.doi.org/10.1088/1361-648X/ac8fd2.

[44] M.G. Vergniory, T.V. Menshchikova, I.V. Silkin, Y.M. Koroteev, S.V. Eremeev, E.V. Chulkov, Electronic and spin structure of a family of Sn-based ternary topological insulators, Phys. Rev. B 92 (2015) 045134, http://dx.doi.org/10.1103/PhysRevB.92.045134, URL https://link.aps.org/doi/10.1103/PhysRevB.92.045134.

[45] M. Bosnar, A. Vyazovskaya, I. Sklyadneva, S.V. Eremeev, Y.M. Koroteev, E.K. Petrov, R. Heid, R.M. Geilhufe, A. Ernst, E.V. Chulkov, M.M. Otrokov, Family of dual topological materials $XSb_4Te_4 (X = Ge, Sn, Pb)$, Phys. Rev. Mater. 9 (2025) 014201, http://dx.doi.org/10.1103/PhysRevMaterials.9.014201, URL https://link.aps.org/doi/10.1103/PhysRevMaterials.9.014201.

[46] L. Fu, C.L. Kane, Topological insulators with inversion symmetry, Phys. Rev. B 76 (2007) 045302, http://dx.doi.org/10.1103/PhysRevB.76.045302, URL https://link.aps.org/doi/10.1103/PhysRevB.76.045302.

[47] C. Pauly, G. Bihlmayer, M. Liebmann, M. Grob, A. Georgi, D. Subramaniam, M.R. Scholz, J. Sánchez-Barriga, A. Varykhalov, S. Blügel, O. Rader, M. Morgenstern, Probing two topological surface bands of Sb_2Te_3 by spin-polarized photoemission spectroscopy, Phys. Rev. B 86 (2012) 235106, http://dx.doi.org/10.1103/PhysRevB.86.235106, URL https://link.aps.org/doi/10.1103/PhysRevB.86.235106.

[48] D. Hsieh, Y. Xia, D. Qian, L. Wray, F. Meier, J.H. Dil, J. Osterwalder, L. Patthey, A.V. Fedorov, H. Lin, A. Bansil, D. Grauer, Y.S. Hor, R.J. Cava, M.Z. Hasan, Observation of time-reversal-protected single-Dirac-cone topological-insulator states in Bi_2Te_3 and Sb_2Te_3, Phys. Rev. Lett. 103 (2009) 146401, http://dx.doi.org/10.1103/PhysRevLett.103.146401, URL https://link.aps.org/doi/10.1103/PhysRevLett.103.146401.

[49] R.J. Cava, H. Ji, M.K. Fuccillo, Q.D. Gibson, Y.S. Hor, Crystal structure and chemistry of topological insulators, J. Mater. Chem. C 1 (19) (2013) 3176–3189, http://dx.doi.org/10.1039/C3TC30186A.

[50] D.O. Scanlon, P.D.C. King, R.P. Singh, A. de la Torre, S.M. Walker, G. Balakrishnan, F. Baumberger, C.R.A. Catlow, Controlling bulk conductivity in topological insulators: Key role of anti-site defects, Adv. Mater. 24 (16) (2012) 2154–2158, http://dx.doi.org/10.1002/adma.201200187.

[51] T. Bathon, S. Achilli, P. Sessi, V.A. Golyashov, K.A. Kokh, O.E. Tereshchenko, M. Bode, Experimental realization of a topological p–n junction by intrinsic defect grading, Adv. Mater. 28 (11) (2016) 2183–2188, http://dx.doi.org/10.1002/adma.201504771.

[52] T. Zhu, L. Hu, X. Zhao, J. He, New insights into intrinsic point defects in V_2VI_3 thermoelectric materials, Adv. Sci. 3 (7) (2016) 1600004, http://dx.doi.org/10.1002/advs.201600004.

[53] M.-H. Du, J. Yan, V.R. Cooper, M. Eisenbach, Tuning Fermi levels in intrinsic antiferromagnetic topological insulators MnBi2Te4 and MnBi4Te7 by defect engineering and chemical doping, Adv. Funct. Mater. 31 (3) (2021) 2006516, http://dx.doi.org/10.1002/adfm.202006516.

[54] M. Lewin, L. Mester, T. Saltzmann, S.-J. Chong, M. Kaminski, B. Hauer, M. Pohlmann, A.M. Mio, M. Wirtssohn, P. Jost, M. Wuttig, U. Simon, T. Taubner, Sb_2Te_3 growth study reveals that formation of nanoscale charge carrier domains is an intrinsic feature relevant for electronic applications, ACS Appl. Nano Mater. 1 (12) (2018) 6834–6842, http://dx.doi.org/10.1021/acsanm.8b01660.

[55] I. Rajput, D. Kumar, A. Lakhani, Empirical role of crystalline defects in the transport properties of Sb_2Te_3 single crystals, Cryst. Growth Des. 23 (8) (2023) 6019–6024, http://dx.doi.org/10.1021/acs.cgd.3c00558.

[56] S. Shimizu, R. Yoshimi, T. Hatano, K.S. Takahashi, A. Tsukazaki, M. Kawasaki, Y. Iwasa, Y. Tokura, Gate control of surface transport in MBE-grown topological insulator $(Bi_{1-x}Sb_x)_2Te_3$ thin films, Phys. Rev. B 86 (2012) 045319, http://dx.doi.org/10.1103/PhysRevB.86.045319, URL https://link.aps.org/doi/10.1103/PhysRevB.86.045319.

[57] M.D. Anoop, J. Yadav, N. Yadav, R. Singh, K. Shinzato, S.N. Dolia, A. Jain, T. Ichikawa, M. Kumar, Effect of isovalent substitution on the structural and electrical properties of $Bi_xSb_{2-x}Te_3$ topological insulator single crystals, Mater. Today: Proc. 31 (2020) 616–621, http://dx.doi.org/10.1016/j.matpr.2019.12.038.